Maximization of No-Load Density in Surface Mounted Permanent Magnet Motor

Frédéric Dubas, Christophe Espanet, A. Miraoui

Maximization of No-Load Flux Density in Surface Mounted Permanent Magnet Motors

F. Dubas, C. Espanet and A. Miraoui.

Research Laboratory in Electronics, Electrical engineering and Systems (LEES), which is a joint Research Unit of the University of Technology of Belfort-Montbéliard (UTBM) and the University of Franche-Comté (UFC) with the INRETS.
LEES-UTBM (Bat.F), Rue Thierry MIEG, F90010 Belfort.
Phone: +33.03.84.58.36.29, Fax: +33.03.84.58.36.36, E-mail: first name.name@utbm.fr

***Abstract* — An exact two-dimensional (2-D) analytical model (AM) of slotless permanent magnet (PM) machines in polar coordinates is used to determine the analytical equations of the air-gap flux density at no-load operation. The authors show that, for a radial magnetization, there is an optimal magnet thickness which permits to maximize the no-load flux density. In order to use easily and directly this optimal value during the design of surface mounted PM motors (SMPMM), the authors propose an original analytical expression of this maximum magnet thickness that have been obtained by interpolation of the values given by several analytical computations. This interpolation function could be applied to SMPMM having a parallel or radial magnetization direction.**

***Index Terms* — Numerical interpolation, no-load air-gap flux density, magnet thickness, parallel and radial magnetization, synchronous permanent magnet machines.**

I. INTRODUCTION

THE magnet thickness is a significant parameter for all the PM machines, since it influences the efficiency, the demagnetization withstand and the cost. Generally, in the optimization processes of the PM machines, one always tries to minimize the magnet thickness, in order to minimize the cost of the motor and, at the some time, the thickness must be higher than a minimal magnet thickness imposed to avoid demagnetizing armature reaction field. However this last optimization criterion is not enough. It could be more interesting to choose the magnet thickness between the demagnetization limit and the maximal limit obtained by maximizing the no-load air-gap flux density. Indeed, from a 2-D polar coordinate AM, which includes both parallel and radial magnetization [1], it is shown that, for a radial magnetization, if the magnet thickness is higher than a particular value, the air-gap flux density decreases. It means that a given value of the flux density can be obtained with two solutions of the magnet thickness, i.e., a small and a large value. From the optimization procedure point of view, this could create difficulties. Since the optimization processes are such that all possible combinations of parameters are considered, the largest value of the magnet thickness can be chosen leading to an unnecessary increase of the weight and the cost. Then, this solution must be discarded and thus, it is necessary to know the maximal magnet thickness which gives the maximum no-load flux density in the air-gap. Therefore, the authors propose an original analytical expression of this maximum magnet thickness. This expression is obtained by interpolation of several values of optimal thickness computed for various geometrical structures. This original analytical expression is a generalized equation contrary to [2] which did not take into account of the influence of magnet pole-arc to pole-pitch ratio on the evolution of the maximum magnet thickness. This interpolation function can be applied to the SMPMM having both parallel and radial magnetization direction. The analytical results are compared with the ones obtained by a numerical analysis using the finite-element method (FEM) [3].

II. A 2-D ANALYTICAL MODEL IN POLAR COORDINATES

A 2-D polar coordinate AM of the SMPMM is used, considering the simplified geometry of Figure 1. The main assumptions are: **1)** End effects are ignored; **2)** The permeability of both stator and rotor are assumed infinite – The saturation effects of the armatures are neglected; **3)** The conductivities of all regions of the model are assumed to be null; **4)** The permanent magnets have a linear demagnetization characteristic, and are fully magnetized in the magnetization direction; **5)** The effects of the slotting are neglected, but the air-gap is increased by applying the classical Carter's coefficient.

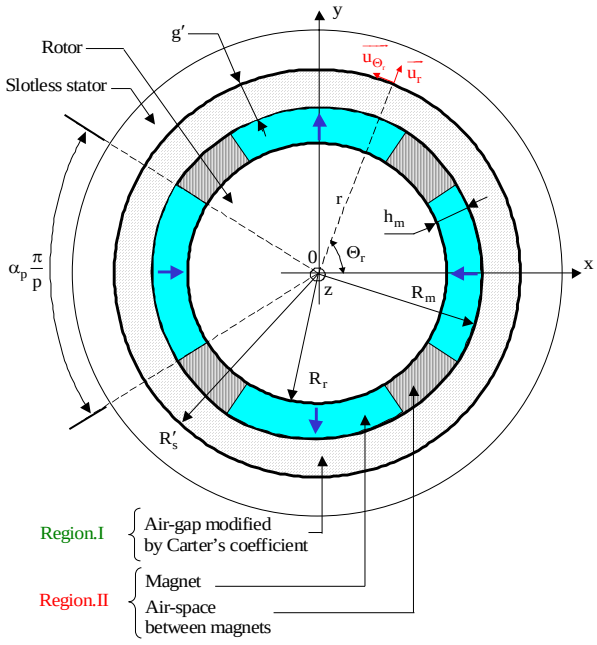

Figure 1. Typical 4-Pole slotless SMPMSM.

The developed 2-D AM in polar coordinates is completely detailed in [1]. This model includes both parallel and radial magnetization. It enables the no-load flux density to be obtained from the solution of the Laplace/Poisson's equations by Fourier's series in two regions: the Region.I, which is the air-gap modified by Carter's coefficient, and the Region.II, which includes the magnets and the air-spaces between magnets. The developed model differs from the model given in [4] because the rotor is transformed into an equivalent rotor, where the relative magnetic permeability of Region.II, μ_{rII}, equals to one and the remanent flux density of the magnet, B_{rm}, is corrected to minimize the error induced by the homogeneity of the relative magnetic permeability in Region.II [5]-[6]. The no-load flux density, in each region, has been compared to the FEM calculations, and the agreement was quite satisfying. The no-load flux density magnitude in the air-gap, i.e., in Region.I, $R_m \le r \le R'_s$, can be expressed as:

$$B^{\mathbf{i}}_{Iv} = B_{rmc}(T_a) \cdot f^{\mathbf{i}}_{Iv\_n}\left(\frac{R_m}{R'_s}, \frac{R_r}{R'_s}, \frac{R_r}{R_m}, \alpha_p, p, n, r, \Theta_r\right). \forall p. \quad (1)$$

where:

- $\mathbf{i}$ is the index of the magnetization direction ($\mathbf{i} \Rightarrow$ P : Parallel or $\mathbf{i} \Rightarrow$ R : Radial),
- $f^{\mathbf{i}}_{Iv\_n}$ is a function in Fourier's series which depend on the variables listed in the brackets. These variables are: R'_s, the inner stator radius modified by Carter's coefficient, R_m, the outer magnet radius, R_r, the inner magnet radius, α_p, the magnet pole-arc to pole-pitch ratio, p, the number of pole-pairs, n, the harmonics number, r, the radial position, and Θ_r, the mechanical angular position of the rotor (the position $\Theta_r = 0$ rad. is in the center of a North magnet).
- B_{rmc} represents the corrected remanent flux density of the magnet at the operating temperature T_a [1]:

$$B_{rmc}(T_a) = k_m \cdot B_{rm0} \cdot \left[1 + \Delta B_{rm} \cdot (T_a - T_{a0})\right]. \quad (2)$$

where k_m is a correction coefficient of the magnet, ΔB_{rm} the remanent flux density variation of the magnet when the temperature rises 1K, T_{a0} the ambient temperature of the magnet, and B_{rm0} the remanent flux density of the magnet at the temperature T_{a0}.

III. AN ORIGINAL ANALYTICAL EXPRESSION OF THE MAXIMUM MAGNET THICKNESS

A. Existence of the Maximum Magnet Thickness

1) Identification of Parameters

From equation (1), we can easily note that the equation (2) only have an influence on the amplitude of the no-load flux density in Region.I. Therefore, considering a linear model, the physical parameters of the magnets have no influence on the maximum magnet thickness, i.e., $h_{m_{max}}$. On the other hand the function in Fourier's series, $f^{\mathbf{i}}_{Iv\_n}$, which depend on the magnets magnetization direction and the geometrical parameters, has an influence on the shape of the no-load flux density in Region.I.

The equation describing the geometrical structure of the slotless SMPMM is defined by:

$$R_r(R'_s, g', h_m) = R_m(R'_s, g') - h_m = R'_s - g' - h_m. \quad (3)$$

where g' is the air-gap modified Carter's coefficient and h_m is the radial thickness of the magnet.

Introducing this above equation into the function $f^{\mathbf{i}}_{Iv\_n}$, we can notice that the key parameters are: α_p, p, the ratios of R_m/R'_s and h_m/R'_s which depend on R'_s, g' and h_m [7].

2) Analysis of the No-Load Flux Density in Region.I

In this analysis, the operating temperature T_a is equal to 100°C and the considered magnet has the following physical parameters: $B_{rm0} = 1.08$ T for $T_{a0} = 20$ °C, $\Delta B_{rm} = -0.12$ %/K and $\mu_{rm} = 1.029$.

Figures 2 and 3 show the evolution of the no-load flux density in Region.I at the surface of the slotless stator according to h_m for $p = 1$, $\alpha_p = 1$, various values of g' and two values of R'_s completely opposed: 10 mm in the first case and 800 mm in the second case ; these two values represent a very small and a very large slotless SMPMSM respectively. These curves have been plotted considering the two possible magnetization directions. We can observe that for parallel magnetization the maximum no-load flux density in Region.I corresponds to the geometrical limit of the machine, i.e., $R'_s \le R_r + h_m + g'$. This geometrical limit is represented by a rotor armature without a back-iron which is not a realistic solution. On the other hand, for a radial magnetization, one can remark that above a given value of h_m, the no-load flux density decreases. This may be surprising but this reduction is due to the leakages between the two magnets. It can be understood by plotting the flux lines between two consecutive magnets. For a given value of g', these leakages increase with h_m [7]. The length of g' also has an influence on the maximal value of the no-load flux density in Region.I. This is mainly due to the leakages around the edge of the magnets, which increase with g' [8]. These different leakages of magnets are represented in Figures 4 and 5 for the two magnetization directions and two particular given geometrical structures, e.g., $p = 1$, $\alpha_p = 1$, $R'_s = 10$ mm, $h_m = 5$ mm, and $g' = 1$ mm or $g' = 3$ mm.

In conclusion, there is a maximal radial thickness of the magnet, which gives a maximum level of no-load flux density in Region.I.

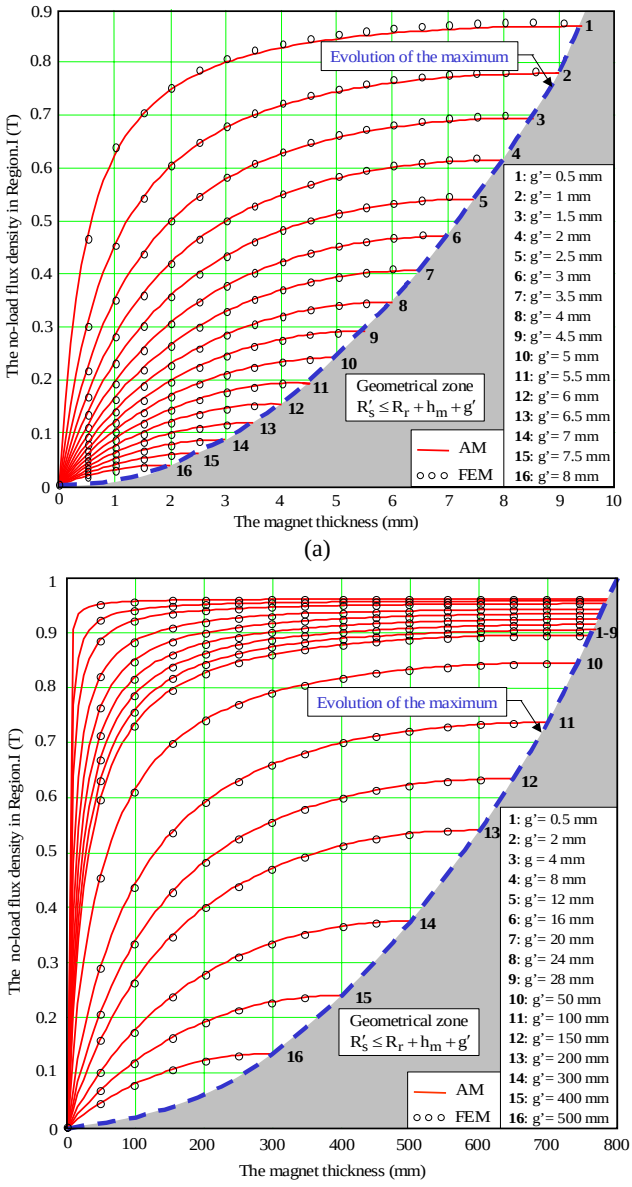

Figure 2. The evolution of B^{i}_{Iv} at the surface of the slotless ($r = R'_s$ and $\Theta_r = 0$ rad.) according to h_m for a **parallel** magnetization, various values of g', $p = 1$, $\alpha_p = 1$ and (a) $R'_s = 10$ mm, (b) $R'_s = 800$ mm.

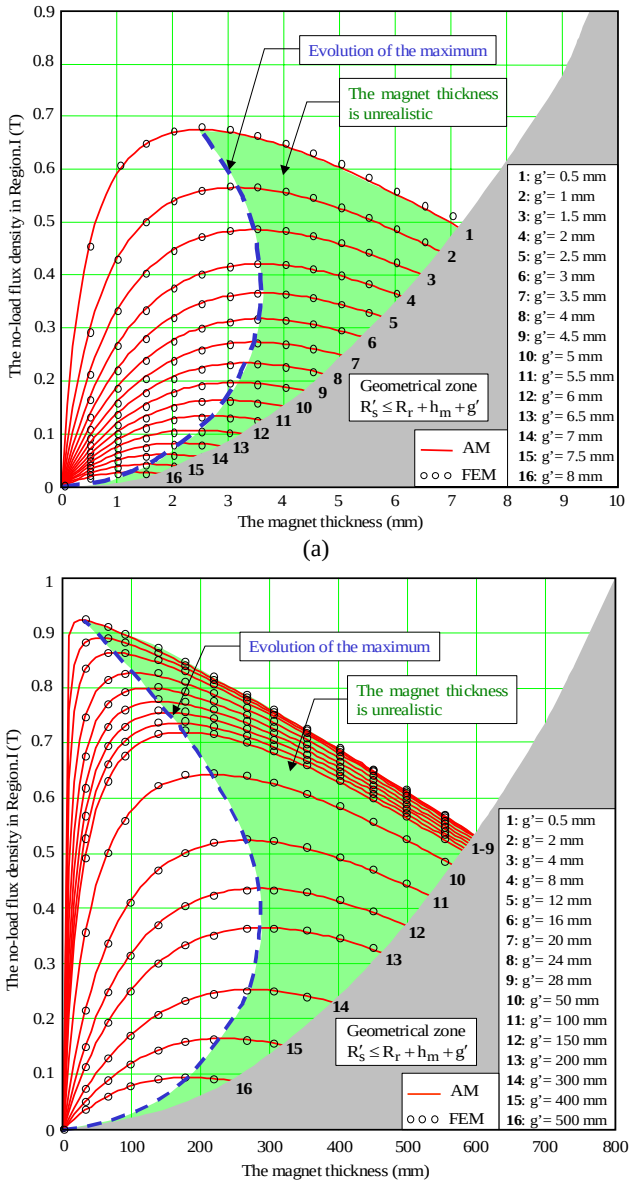

Figure 3. The evolution of B^{i}_{Iv} at the surface of the slotless ($r = R'_s$ and $\Theta_r = 0$ rad.) according to h_m for a **radial** magnetization, various values of g', $p = 1$, $\alpha_p = 1$ and (a) $R'_s = 10$ mm, (b) $R'_s = 800$ mm.

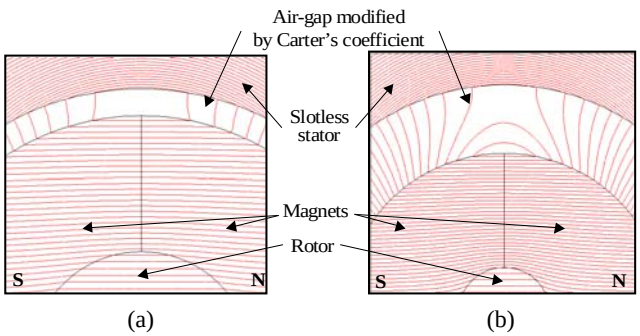

Figure 4. The different flux leakages between the magnets for a **parallel** magnetization and two given geometries – $p = 1$, $\alpha_p = 1$, $R'_s = 10$ mm, $h_m = 5$ mm, and (a) $g' = 1$ mm, (b) $g' = 3$ mm.

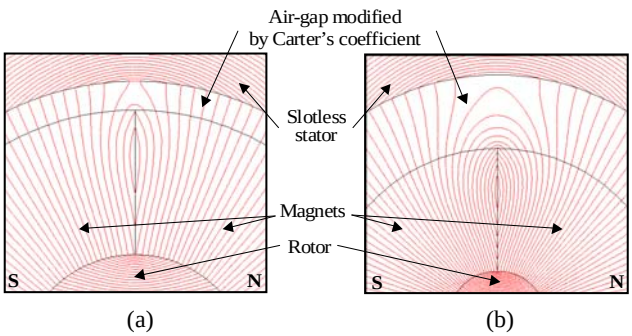

Figure 5. The different flux leakages between the magnets for a **radial** magnetization and two given geometries – $p = 1$, $\alpha_p = 1$, $R'_s = 10$ mm, $h_m = 5$ mm, and (a) $g' = 1$ mm, (b) $g' = 3$ mm.

B. Interpolation of the Maximum Magnet Thickness

1) Problematic

If the 2-D polar coordinate AM of the SMPMM is used with a radial magnetization to achieve an optimal design, this could lead a bad solutions. Indeed, in particular case, two different values of h_m can lead to the same value of no-load flux density. The highest solution of h_m, which can be unrealistic, must be discarded and thus there is a need to know the value of $h_{m_{max}}$ for a given geometry. It is then interesting to have an analytical expression of $h_{m_{max}}$. But it is not possible to find an symbolic solution of the equation $dB_{Iv}^{i}/dh_m = 0$. Therefore, we proposed to interpolate an original analytical expression of $h_{m_{max}}$ as a function of the considered parameters.

In Figure 6, the no-load flux density in Region.I is plotted versus h_m for the two magnetization directions, two values of p (namely 1 and 12) and a given geometrical structure, e.g., $\alpha_p = 1$, $R'_s = 10$ mm and $g' = 1$ mm. We can see that the magnetization direction of the magnets does not have almost any more influence on the no-load flux density in Region.I, when p is high [8].

Figures 7 show the saturation effects on the evolution of the maximum for a given geometrical structure, e.g., $p = 1$, $\alpha_p = 1$, $R'_s = 10$ mm, $h_m = 5$ mm and $g' = 1$ mm. In this analysis, the materials of the magnetic circuit, i.e., stator and rotor, have a saturation flux density, B_{sat}, of 1.75 T and a relative magnetic permeability to the origin, μ_{r0}, of 8639. In Figure 7(a) and 7(b), we can remark that the saturation of the materials causes an increase of the leakages around the edge of the magnets for the two magnetization directions. In Figure 7(c), we can then observe that with the effects saturation, the maximum no-load flux density in Region.I begins to disappear in order to approach the geometrical limit of the machine.

These notes and the geometrical limit for a parallel magnetization (Figure 2) lead us to use a radial magnetization to determine the analytical expression of $h_{m_{max}}$. And the saturation effects will not be taken into account in this interpolation function.

2) Numerical Approximation

By using the computed values of this maximum, we can evaluate the ratio of $h_{m_{max}}/R'_s$ versus the ratio of R_m/R'_s. Figures 8(a) and 8(b) show the evolution of these standardized magnet curves for various values of p (namely 1 to 12) with $\alpha_p = 1$ and for various values of α_p (namely 0.1 to 1) with $p = 1$ respectively. We can notice that, whatever p and α_p, R'_s doesn't have any influence on the shape of standardized magnet curves, contrary to p and α_p which decrease them.

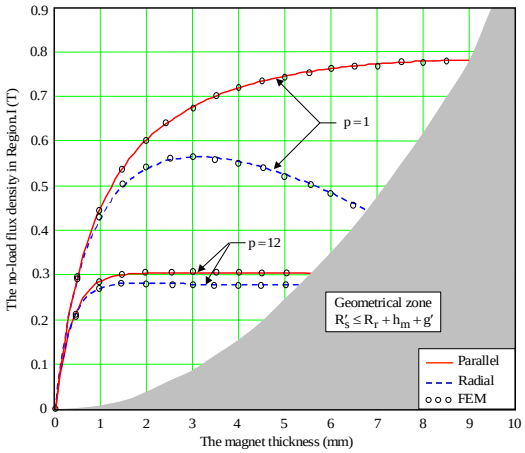

Figure 6. Influence of B_{Iv}^{i} with h_m for two magnetization direction, for two values of p and for a given geometry – $\alpha_p = 1$, $R'_s = 10$ mm and $g' = 1$ mm.

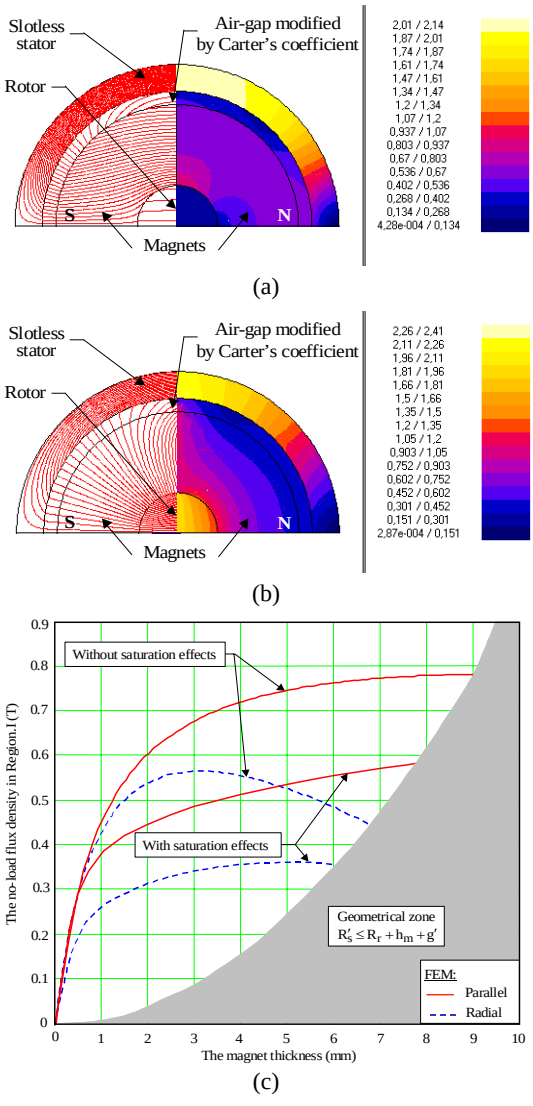

Figure 7. The saturation effects for a given geometry – $p = 1$, $\alpha_p = 1$, $R'_s = 10$ mm, $h_m = 5$ mm and $g' = 1$ mm: The flux lines and color shade for (a) a **parallel** magnetization, (b) a **radial** magnetization ; and (c) The evolution of B_{Iv}^{i} at the surface of the slotless ($r = R'_s$ and $\Theta_r = 0$ rad.) according to h_m.

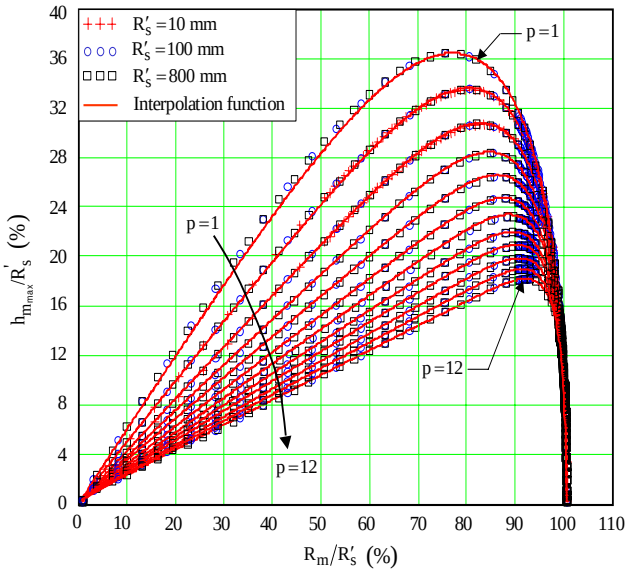

(a)

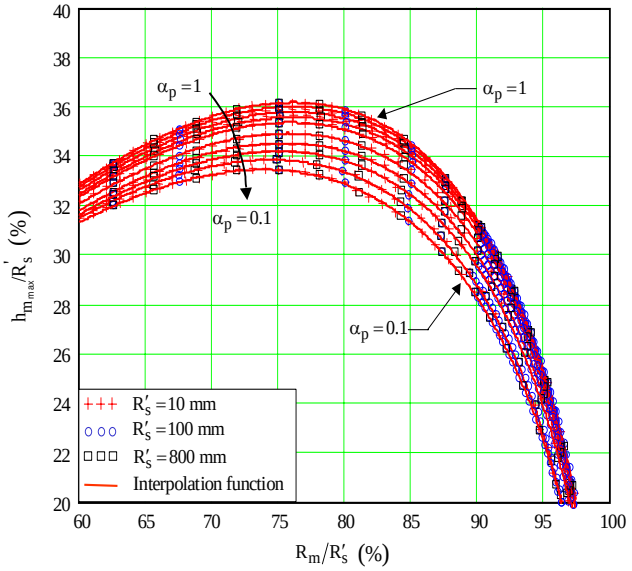

(b)

Figure 8. Evolution of $h_{m_{max}}/R'_s$ with R_m/R'_s for various values of R'_s and (a) p with $\alpha_p = 1$, (b) α_p with $p = 1$.

To be able to take into account this phenomenon in a design model, a numerical approximation was done. An original analytical expression of $h_{m_{max}}$ is proposed [2]:

$$h_{m_{max}} = f_1(p) \cdot R'_s \cdot \left(\frac{R_m}{R'_s}\right)^{g_1(\alpha_p)} \cdot \left[1 - \left(\frac{R_m}{R'_s}\right)^{f_2(\alpha_p, p)}\right]^{g_2(\alpha_p)} \quad . (4)$$

where f_1, f_2, g_1 and g_2 are the interpolation functions of $h_{m_{max}}$ which depend on α_p or p, but also on the coefficients m_1, m_2,..., m_7 and n_1, n_2,..., n_{12}. The coefficients m_k and n_j of the interpolation functions are determined for various values of p (namely 1 to 12) with $\alpha_p = 1$ and for various values of α_p (namely 0.1 to 1) with $p = 1$ respectively. These coefficients will be evaluated by applying a non-linear method, of Levenberg-Marquardt type, in order to minimize the error between the function and the points calculated by the analytical model. The expressions and the evolutions of these interpolation functions, the values of these coefficients and the interpolation errors are given in the Appendix.

Thanks to this original analytical expression, it is possible to determine of $h_{m_{max}}$ for a given geometrical structure with an total interpolation error lower than 2.264%.

IV. CONCLUSION

In this paper, an original analytical expression of the maximum magnet thickness has been proposed. Indeed, the authors have shown that there is effectively a maximum magnet thickness which enables to reach a maximum no-load flux density in the air-gap. The 2-D polar coordinate AM of the SMPMM and the interpolated function of the maximum magnet thickness both permit now to eliminate the too heavy and expensive solutions and to maximize the no-load flux density in the air-gap at the same time.

REFERENCES

[1] F. Dubas, C. Espanet, and A. Miraoui, "Analytical Modeling of No-Load Flux Density in Surface Mounted Permanent Motors", *International Agean Conference on Electrical Machines (ACEMP 04)*, pp. 283-290, 26-28 May 2004, İstanbul, TÜRKIYE.

[2] F. Dubas, C. Espanet, and A. Miraoui, "Maximization of No-Load Flux Density in Surface Mounted Permanent Magnet Motors", *Conference on Electromagnetic Field Computation (CEFC 04)*, pp. 202, 6-9 June 2004, Seoul, KOREA.

[3] FLUX2D, "Notice d'utilisation générale", Version7.5. Cedrat S.A Electrical Engineering, 10 Chemin de pré carré, Zirst, 38246 Meylan, FRANCE.

[4] Z.Q. Zhu, D. Howe, and C.C. Chan, "Improved Analytical Model for Predicting the Magnetic Field Distribution in Brushless Permanent Magnet Machines", *IEEE Transactions on Magnetics*, vol. 35, no. 1, pp. 229-238, January 2002.

[5] N. Boules, "Prediction of No-Load Flux Density Distribution in Permanent Magnet Machines", *IEEE Transactions on Industry Applications*, vol. IA-21, no. 4, pp. 633-643, May/June 1985.

[6] C. Espanet, "Modelisation et conception optimale de moteurs sans balais à structure inverse. Application au moteur-roue", *Thesis*, January 1999, University of Franche-Comté (UFC), Belfort, FRANCE.

[7] J. Engström, "Analysis and Verification of a Slotless Permanent Magnet Motor for high Speed Applications", Royal Institute of Technology, Department of Electrical Engineering, *Electrical Machines and Power Electronics*, Stockholm 2001.

[8] T. Sebastian, and V. Gangla, "Analysis of Induced EMF Waveforms and Torque Ripple in a Brushless Permanent Magnet Machine", *IEEE Transactions on Industry Applications*, vol. 32, no. 1, pp. 195-200, January/February 1996.

APPENDIX

The interpolation functions of $h_{m_{max}}$ for various values of p (namely 1 to 12) with $\alpha_p = 1$:

$$f_1(p) = m_1 \cdot \exp\left(-m_2 \cdot p^{m_3}\right) + m_4. \quad \text{(A1)}$$

$$f_2(\alpha_p, p) = g_3(\alpha_p) \cdot \exp\left(m_5 \cdot p^{m_6}\right) + m_7. \quad \text{(A2)}$$

The values of the coefficients m_k:

$$\begin{bmatrix} m_1 \\ m_2 \\ m_3 \\ m_4 \\ m_5 \\ m_6 \\ m_7 \end{bmatrix} = \begin{bmatrix} 0.948 \\ 0.572 \\ 0.465 \\ 0.046 \\ 2.181 \\ 0.275 \\ 2.934 \times 10^{-5} \end{bmatrix}. \quad \text{(A3)}$$

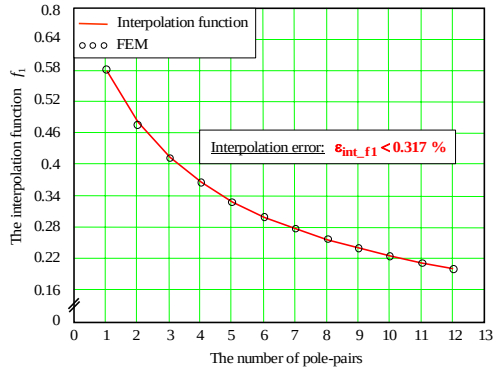

(a)

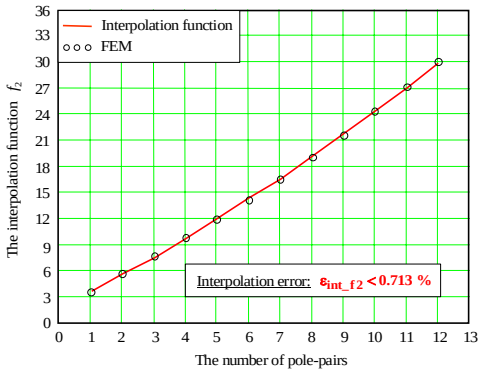

(b)

Figure A.1. The interpolation functions $f_1(p)$ and $f_2(\alpha_p, p)$ of $h_{m_{max}}$ for various values of p with $\alpha_p = 1$.

The interpolation functions of $h_{m_{max}}$ for various values of α_p (namely 0.1 to 1) with $p = 1$:

$$g_1(\alpha_p) = n_1 \cdot \exp\left(n_2 \cdot \alpha_p^{n_3}\right) + n_4. \quad \text{(A4)}$$

$$g_2(\alpha_p) = n_5 \cdot \left(\alpha_p^{n_6} - n_7\right)^2 + n_8. \quad \text{(A5)}$$

$$g_3(\alpha_p) = n_9 \cdot \exp\left(n_{10} \cdot \alpha_p^{n_{11}}\right) + n_{12}. \quad \text{(A6)}$$

The values of the coefficients n_j:

$$\begin{bmatrix} n_1 \\ n_2 \\ n_3 \\ n_4 \end{bmatrix} = \begin{bmatrix} 0.2123 \\ 0.071 \\ 1.728 \\ 0.7322 \end{bmatrix}, \begin{bmatrix} n_5 \\ n_6 \\ n_7 \\ n_8 \end{bmatrix} = \begin{bmatrix} 0.1828 \\ 0.7773 \\ 0.5478 \\ 0.4025 \end{bmatrix} \text{ and } \begin{bmatrix} n_9 \\ n_{10} \\ n_{11} \\ n_{12} \end{bmatrix} = \begin{bmatrix} 0.232 \\ 0.41 \\ 1.359 \\ 0.048 \end{bmatrix}. \quad \text{(A7)}$$

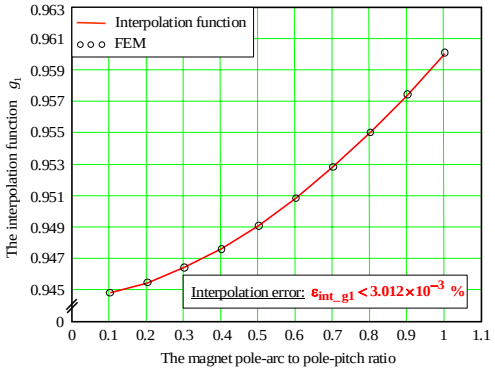

(a)

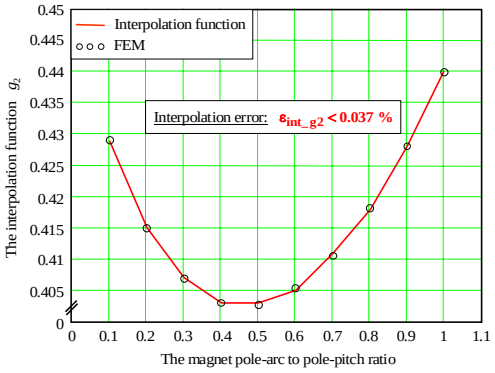

(b)

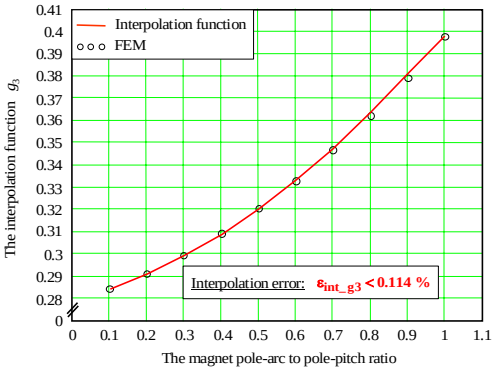

(c)

Figure A.2. The interpolation functions $g_1(\alpha_p)$, $g_2(\alpha_p)$ and $g_3(\alpha_p)$ of $h_{m_{max}}$ for various values of α_p with $p = 1$.